Properties of Josephson Traveling Wave Parametric Amplifier With a Non-Sinusoidal Current-Phase Relation and Resonant Phase Matching

Claudio Guarcello, Carlo Barone, Giovanni Carapella, Giovanni Filatrella, Andrea Giachero, and Sergio Pagano

***Abstract*—A comprehensive numerical analysis of the dynamical response of Josephson Traveling Wave Parametric Amplifiers (JTWPA) under varying driving conditions is presented. The primary goal is to examine the effects of a current–phase relation (CPR) incorporating a second-harmonic contribution. The analysis further investigates how parameters such as pump intensity, signal frequency, and DC bias current influence the transition to chaos. The results reveal a wide range of dynamical regimes in JTWPAs, offering insights into optimizing device performance and stability. Notably, the shape of the CPR is shown to have a significant impact on the operational effectiveness and stability of JTWPAs. To obtain results closer to real devices, numerical modeling of JTWPAs implementing Resonant Phase Matching (RPM) circuitry has been performed. We have verified that the introduction of RPM allows a significant increase in the amplifier gain also in the case of non-sinusoidal CPR. These findings may have important implications for the development of next-generation JTWPAs, which are essential components in quantum computing and precision measurement applications.**

***Index Terms*—Josephson junctions, parametric amplifiers, quantum-noise limited amplifiers, superconducting microwave devices.**

Received 10 October 2025; revised 30 December 2025 and 19 January 2026; accepted 20 January 2026. Date of publication 26 January 2026; date of current version 4 February 2026. This work was supported in part by PNRR MUR Projects PE0000023, in part by NQSTI under Grant H43C22000870001, in part by NBJTWPA under Grant H43C22000870001 QSENS, in part by the Italian Institute of Nuclear Physics (INFN) QUARTET, and in part by the University of Salerno Italy under Grant FRB22PAGAN, Grant FRB23BARON, and Grant FRB24CAVAL. *(Corresponding author: Sergio Pagano.)*

Claudio Guarcello and Giovanni Carapella are with the Physics Department, University of Salerno, 84084 Fisciano, Italy, and also with the Gruppo Collegato di Salerno, Istituto Nazionale di Fisica Nucleare, 84084 Fisciano, Italy (e-mail: cguarcello@unisa.it; gcarapella@unisa.it).

Carlo Barone and Sergio Pagano are with the Physics Department, University of Salerno, 84084 Fisciano, Italy, and with the Gruppo Collegato di Salerno, Istituto Nazionale di Fisica Nucleare, 84084 Fisciano, Italy, and also with the Salerno Unit, C.N.R. SPIN Institute, 84084 Fisciano, Italy (e-mail: cbarone@unisa.it; spagano@unisa.it).

Giovanni Filatrella is with the Science and Technology Department, University of Sannio, 82100 Benevento, Italy (e-mail: filatr@unisannio.it).

Andrea Giachero is with the Physics Department, University of Milano Bicocca, 20126 Milano, Italy, and with the Milano Bicocca Section, Istituto Nazionale di Fisica Nucleare, 00186 Milano, Italy, and also with the Bicocca Quantum Technologies (BiQuTe) Centre, 20126 Milano, Italy (e-mail: andrea.giachero@unimib.it).

Color versions of one or more figures in this article are available at https://doi.org/10.1109/TASC.2026.3658055.

Digital Object Identifier 10.1109/TASC.2026.3658055

I. Introduction

AMPLIFYING weak microwave signals for the readout of superconducting qubits or for interfacing quantum detectors is essential for applications in quantum computing, basic physics experiments, and radio astronomy. The best low-noise microwave amplifiers reach the quantum-noise limit by working at very low temperatures and using parametric pumping in circuits with Josephson junctions (JJs) or superconducting elements with high kinetic inductance [1]. Among superconducting parametric amplifiers, Josephson Traveling Wave Parametric Amplifiers (JTWPAs) offer large bandwidth, high gain, and high saturation power, at the expense of a rather complex structure with many elements [2], [3], [4], [5], [6]. This complexity may result in unwanted effects, such as signal reflection, oscillation, spurious harmonic generation, and even chaotic behavior [7].

Proper modelling of the dynamical system forming a JTWPA, without simplifying approximations is, therefore, a crucial aspect. Moreover, as parametric amplifiers increasingly rely on unconventional weak links with high transparency, and hence non-sinusoidal current–phase relations (CPRs), [8] it becomes important to develop JTWPA descriptions that capture CPR harmonics and their impact on the device nonlinearity.

II. The Josephson Traveling Wave Parametric Amplifier

A JTWPA is a transmission line composed of many cells, each containing one or more JJs, the nonlinear elements. Among the various possibilities, we focused on a cell made of a loop formed by a JJ and a superconducting inductor (forming an RF-SQUID cell), and with a capacitor to ground, see Fig. 1. The JJ is modeled, following the standard Resistively Shunted Junction (RSJ) model, as the parallel combination of a "pure" Josephson element, a capacitor C_{J} and a resistor R_{J} (here we used $R_{\mathrm{J}} = 20\ \mathrm{k}\Omega$) [9], [10], [11]. The current flowing through and voltage across each JJ are then given by:

$$I = I_{\mathrm{J}} + I_{R_{\mathrm{J}}} + I_{C_{\mathrm{J}}} \tag{1}$$

and

$$V = \frac{\Phi_0}{2\pi}\frac{d\varphi}{dt}, \tag{2}$$

where $\Phi_0 \simeq 2.07\,10^{-15}$ W is the flux quantum, φ is the quantum phase difference across the junction, and $I_{\mathrm{J}}(\varphi)$ is the CPR of the "pure" Josephson element, that can assume different forms [12], [13]:

$$\text{standard}: \qquad I_J(\varphi) = I_c \ \sin(\varphi) \tag{3}$$

$$\text{transparency dependent}: I_J(\tau,\varphi) = I_c\ \alpha \frac{\tau \sin(\varphi)}{2\sqrt{1-\tau\ \sin(\varphi)^2}} \tag{4}$$

$$\text{second harmonic}: \qquad I_J(\varphi) = I_c\ \alpha\ (J_{c1}\sin(\varphi) + J_{c2}\sin(2\varphi)) \tag{5}$$

Here I_c is JJ critical current (i.e., the maximum dc current that can flow in the junction while maintaining the zero-voltage state), τ is the transparency skewness parameter, α is a scaling parameter chosen such that $\max_{\varphi} I_{\mathrm{J}}(\varphi) = I_c$, J_{c1} and J_{c2} are the relative weights of the first and second harmonic respectively.

The different CPR can be a result of the materials forming the junction, its geometrical shape, and, also, the temperature [14], [15], [16], [17], [18], [19]. Normally, a "*standard*", i.e., sinusoidal, CPR is used to model a JTWPA. However, as more research is done in improving the device performances, the presence of a nonstandard CPR cannot be excluded. JTWPAs made with junctions having a CPR with variable transparency have been investigated in [20], where it is found that the device response is highly sensitive to the specific form of the CPR. Increasing its skewness leads to a reduction of the maximum achievable gain, while at the same time enlarging the range of pump intensities over which the system remains stable. Moreover, the onset of chaotic dynamics becomes considerably sharper at higher skewness.

A second-harmonic CPR has been shown to accurately describe superconducting junctions with ferromagnetic barriers [17], [21], as well as JJs based on semiconductors [22], [23], [24], [25], graphene [26], and unconventional superconductors [27], [28]. Although higher-harmonic contributions are typically negligible in conventional tunnel junctions, recent work has demonstrated that they can also modify the excited-state spectrum of Al- and AlO-based Josephson qubits [29]. Relatedly, microscopic barrier inhomogeneities (e.g., pinholes or weak points) can yield a small set of highly transmissive channels and thereby enhance higher-harmonic contributions even in nominally Al/AlO $_x$ /Al tunnel junctions [30], [31]. Finally, we note a recent mesoscopic theory for JJs formulated within nonrelativistic scalar electrodynamics, in which a CPR including a second-harmonic term arises naturally [32]. More recently, the second-harmonic form of CPR has been explored in the context of JTWPA [33]: by tuning the relative weights of the harmonic CPR components, substantial amplification can be obtained, with gains up to 13 dB even without the implementation of dispersion engineering. Furthermore, it was discussed how non-sinusoidal contributions to the CPR can drive the system from a stable, periodic regime into chaotic dynamics, particularly in the case of $J_{c2} < 0$. We note that additional circuit embedding (e.g., RF-SQUID unit cells) can yield an effective non-sinusoidal current–phase response due to screening and flux-dependent effects; for TWPA implementations and an overview of CPRs associated with different Josephson-based nonlinearities [4], [34]. In this work, however, we focus on the second-harmonic contribution of the CPR at the junction level, which depends on the underlying weak-link physics.

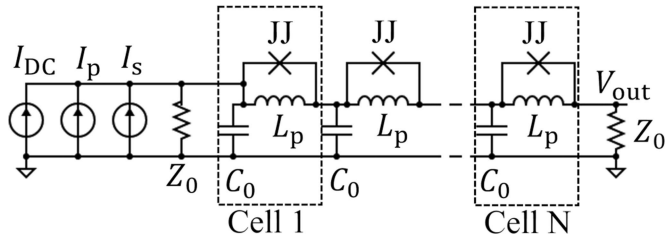

Fig. 1. Equivalent electric circuit of a JTWPA.

As evident in Fig. 1, where the equivalent electric circuit of the investigated JTWPA is shown, the transmission line is made by N cells, each consisting in the parallel of a Josephson junction JJ, a superconducting inductor, L_{p}, and a capacitor C_0 to ground. At the beginning of the line is applied the signal to amplify, I_{s}, the microwave pump tone, I_{p} and an optional DC bias current I_{DC}, used to shift the equilibrium phase of the junctions. Z_0 represents the source and load impedances, typically 50 Ω. The voltage at the $\mathrm{V_{out}}$ port represents the amplified signal, as well as the pump tone and various mixing products. Throughout this work we consider a purely current-biased operation and neglect any externally applied magnetic flux bias, $\Phi_{\mathrm{ext}} = 0$, so that the non-sinusoidal CPR is treated as a junction-level property rather than a topology-induced effect.

Using the Kirckhoff's laws and the constitutive relation of the components, the circuit in Fig. 1 can be easily converted in a set of nonlinear, coupled ordinary differential equations, describing the time evolution of voltages and currents in each part of the circuit. The system of differential equations can then be solved using standard numerical methods [35]. The system's dynamics are obtained by integrating the system of N coupled differential equations, one for each cell of the JTWPA. The time-domain integration is performed with an in-house developed FORTRAN code implementing the implicit finite-difference scheme (tridiagonal solver), while FFT-based spectral post-processing is carried out using the Mathematica [36] software. The chosen normalized time step and integration time are $\Delta t = 0.01$ and $t_{max} = 20000$, respectively. Numerical details are reported in [20]. The Josephson nonlinearity is retained in full through the non-sinusoidal CPR (5), i.e., no small-signal or Taylor expansion of the nonlinear term is employed. Related time-domain multiphysics/FDTD–FEM approaches have recently been reported [37].

The design parameters were chosen to mimic a real device, designed and realized by INRIM-Italy, and are reported in Table I. The JTWPA is biased with a pump tone, with a frequency of 7 GHz and a power ranging from -70 to -45 dBm, and a small signal tone, with a power of -100 dBm and frequency ranging from 4 to 10 GHz. The Fourier spectrum of the output signal at $\mathrm{V_{out}}$ is analyzed using fast FFT algorithms.

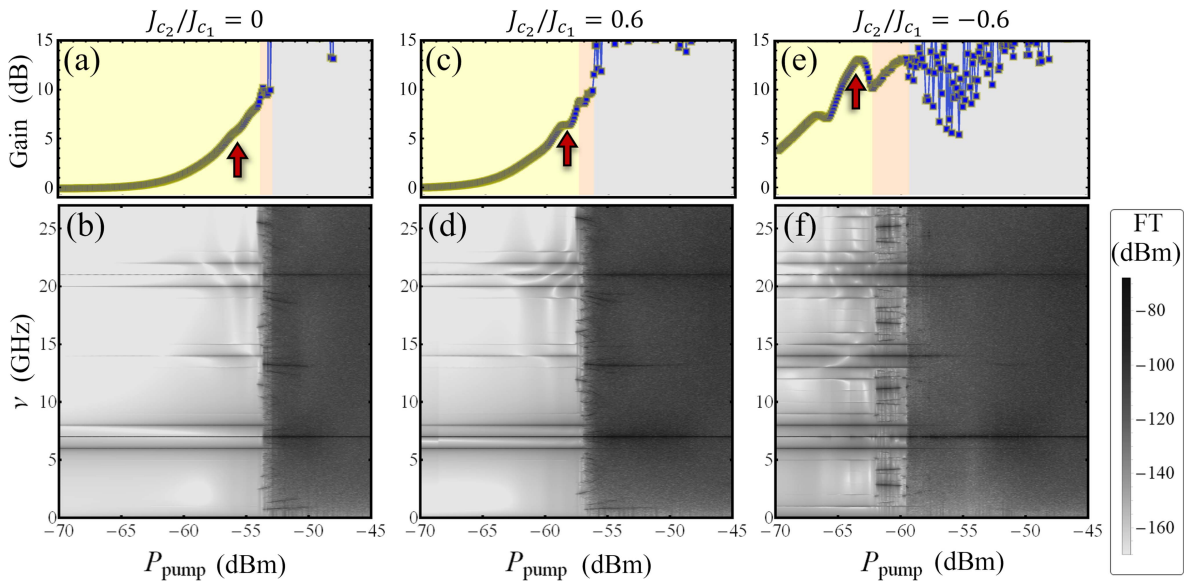

Fig. 2. JTWPA gain (top panels) and output voltage spectrum (bottom panels) *vs* pump power, for different amplitudes of the second-harmonic contribution. Left panel: $J_{c2}/\ J_{c1}$ =0 (pure sinusoidal CPR). Middle panel: $J_{c2}/\ J_{c1}$ =0.6. Right panel: $J_{c2}/\ J_{c1}$ =-0.6. The light-yellow area represents regular behavior with few spectral components, while the pink/gray area a chaotic behavior with large spectral noise. The arrows point to the value chosen for RPM testing. The color scale on the left indicates the signal power in the frequency spectrum.

TABLE I
PARAMETER VALUES USED IN SIMULATIONS

name	N	C_J	R_J	I_c	L_p	C_0	Z_0
Unit		fF	kΩ	μA	pH	fF	Ω
value	990	200	20	2	120	24	50

Fig. 2(a) and (b) show results obtained using a standard CPR. Panel (a) focuses on the signal gain versus the pump tone amplitude: it shows an increasing gain with the pump power. However, for pump power exceeding -54 dBm, the gain jumps from about 10 dB to about 20 dB and is rather unstable. By looking at the spectrum of the output signal, panel (b), it is possible to see a large peak due to the pump (at 7 GHz), smaller peaks due to the amplified signal (at 6 GHz) and the idle tone (at 8 GHz), plus several harmonics and mixing products related to them. These mixing products increase in number and amplitude as the pump power increases up to a transition to a chaotic state for power above -54 dBm. Essentially, by scanning the pump amplitude it is possible to drive the JTWPA from a low gain with clean spectrum state, through a high gain with more harmonics, up to a chaotic state characterized by large noise rise. This effect is visible only by computing the full dynamical solutions of the JTWPA equations. Other methods, employing pre-configured ansatz of the output voltage frequency components [38], [39], [40], although numerically faster, cannot render the full complexity of the system, especially near a chaotic transition.

III. JTWPA WITH SECOND HARMONIC CPR

When considering a modified CPR, like in (5), an additional parameter is introduced, namely the ratio between the second and first harmonic of the CPR: J_{c2}/J_{c1}. This value can range typically from -1 to 1, where 0 means standard CPR, as in (3). In performing the numerical simulation of the system and to be comparable with the pure sinusoidal CPR, for each choice of the J_{c2}/J_{c1} ratio, we have rescaled the α parameter in (5) in such a way that I_c corresponds to the maximum value of $I_J(\varphi)$.

The effect of second-harmonic on the JTWPA dynamics appears quite destabilizing, as it shifts the threshold of chaos to lower pump power levels, see Fig. 2(d)–(f). However, for $J_{c2}/\ J_{c1} = -0.6$, a larger gain is observed for a pump power of -64 dBm, see Fig. 2(e), thus showing that the harmonic component of the CPR is helping to achieve a more efficient energy transfer between the pump and the signal.

To improve the JTWPA gain, limited by the transmission line dispersion that causes a dephasing between pump and signal tones, typically Resonant Phase Matching (RPM) elements are periodically added to the transmission line [39], [41], [42]. These consist of parallel LC resonators connected to ground and capacitively coupled to the transmission line each n cells. The role of the resonators is to change the wavevector of the pump tone, when it is close to their resonance frequency, thus rephasing it with the signal. It has been numerically and experimentally demonstrated that, in this way, a gain larger than 20 dB can be achieved [39], [42]. The question is whether this mechanism is still valid in presence of non-sinusoidal CPR. To check this hypothesis, we have implemented the JTWPA model with RPM elements, tuned at a frequency of 7 GHz. To speed up the model development, and to check the consistency of different numerical modeling schemes, we have implemented the RPM JTWPA using a SPICE schematic simulator: the freely available LTSPICE [43].

We have defined the Josephson element, which is not present in the default libraries of LTSPICE, by means of controlled current sources, a standard SPICE component, and build the

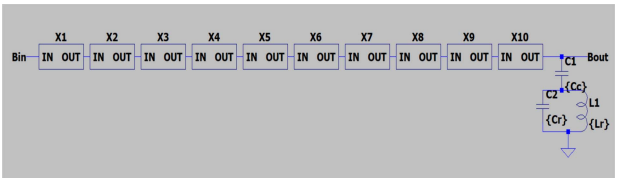

Fig. 3. One of the 99 sections of the RPM JTWPA showing 10 cells, represented by the rectangular blocks, followed by the RPM circuit. The component values are $C_c = C_0 = 24$ fF, $C_r = 3$ pF and $L_r = 170$ pH, resulting in a resonant frequency of 7 GHz.

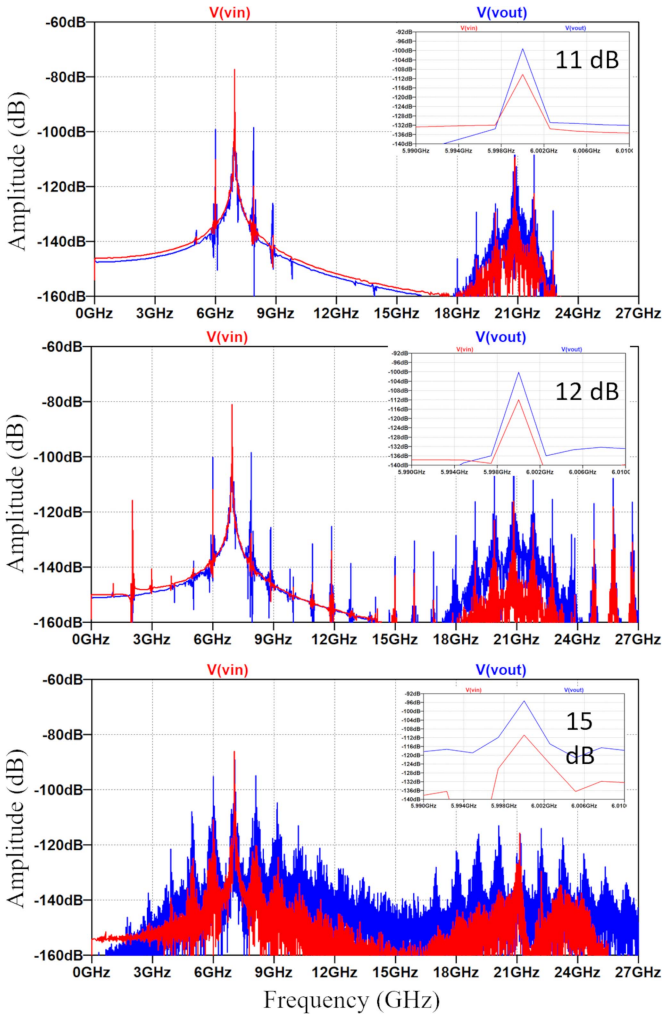

Fig. 4. Frequency spectrum of the input (red) and output (blue) signals from the JTWPA. Top panel: $J_{c2}/J_{c1} = 0$, $F_p = 6.95$ GHz, $P_p = -55$ dBm. Middle panel: $J_{c2}/J_{c1} = 0.6$, $F_p = 6.95$ GHz, $P_p = -58$ dBm. Bottom panel: $J_{c2}/J_{c1} = -0.6$, $F_p = 7.05$ GHz, $P_p = -64$ dBm. Inset: blow up of the spectra at the signal frequencies, showing the gain as ratio between output and input signal, also indicated by the black label. The vertical dB scale is in LTSPICE volt units.

circuit implementing the JTWPA already investigated above. We first checked that, for sinusoidal CPR, the results of the LTSPICE simulation are equivalent to those obtained with the FORTRAN code [20]. These results are not reported here due to space limitation. Then, we implemented the RPM circuitry, which was added every 10 cells. In Fig. 3 one of the 99 sections forming the RPM JTWPA, as visible in the LTSPICE schematic editor, is shown.

By running the time domain simulation of the JTWPA circuit implementing the RPM, we first made a scan to identify the best values for the pump tone frequency, which must be close to the RPM resonant frequency. Then we performed a time domain simulation with the identified frequencies using the same values for J_{c2}/J_{c1} of Fig. 2 and choosing as amplitudes respectively: -55 dBm, -58 dBm and -64 dBm, as indicated by the arrows in Fig. 2.

The resulting output voltage spectra are shown in Fig. 4. In the top panel is shown the effect of RPM addition on a pure sinusoidal CPR. In this case the resulting spectrum is quite clean, with the presence of the pump (F_p), signal (F_s) and idle (F_i) tones at the frequencies corresponding to the 4WM mechanism: ($2\ F_p = F_s + F_i$). Relatively large peaks are also visible in the spectrum at frequencies close to the third harmonic of the pump frequency F_p. Being quite far in frequency, these signals can be easily filtered out in a real device. Overall, the addition of RPM enhances the gain to from 8 dB to 11 dB.

In the middle panel the same situation is represented for the case $J_{c2}/J_{c1} = 0.6$. Here, the spectrum shows many more frequency mixing products extending also at frequencies close to that of the signal, but with reduced amplitudes. The overall gain goes from 7 dB to 12 dB. In the bottom panel the more interesting situation of $J_{c2}/J_{c1} = -0.6$ is shown. The frequency spectrum is much more crowded, even if the pump power Pp is much lower (-64 dBm) with respect to the other two cases. The gain goes from 12 dB to 15 dB, but at the expense of the presence of many mixing products in all the interesting frequency bands for JTWPA applications (4 GHz to 12 GHz).

IV. Conclusion

Direct numerical simulation of JTWPA dynamics can provide insight into the device operation, including unwanted effects. JTWPAs made with Josephson junctions having non-standard CPR show significant changes in the operative parameters, such as maximum gain and chaos transition threshold. The implementation of Resonant Phase Matching circuits improves the JTWPA signal gain also in the case of nonstandard current profiles. However, care must be taken to avoid excessive generations of spurious signals. We emphasize that the present time-domain model is classical and deterministic: the increased spectral 'noise' observed in Fig. 4 reflects nonlinear mixing and/or intermodulation products, while a quantitative assessment of the added (quantum) noise requires a quantum input–output treatment [44] and related JTWPA quantum-noise analyses [45].

References

[1] J. Aumentado, "Superconducting parametric amplifiers: The state of the art in Josephson parametric amplifiers," *IEEE Microw. Mag.*, vol. 21, no. 8, pp. 45–59, Aug. 2020, doi: 10.1109/MMM.2020.2993476.

[2] M. Sweeny and R. Mahler, "A travelling-wave parametric amplifier utilizing Josephson junctions," *IEEE Trans. Magn.*, vol. TMAG-21, no. 2, pp. 654–655, Mar. 1985, doi: 10.1109/TMAG.1985.1063777.

[3] M. T. Bell and A. Samolov, "Traveling-wave parametric amplifier based on a chain of coupled asymmetric SQUIDs," *Phys. Rev. Appl.*, vol. 4, Aug. 2015, Art. no. 024014, doi: 10.1103/PhysRevApplied.4.024014.

[4] A. B. Zorin, "Josephson traveling-wave parametric amplifier with three-wave mixing," *Phys. Rev. Appl.*, vol. 6, 2016, Art. no. 034006, doi: 10.1103/PhysRevApplied.6.034006.

[5] L. Fasolo et al., "Superconducting Josephson-Based Metamaterials for Quantum-Limited Parametric Amplification: A Review," in *Advances in Condensed-Matter and Materials Physics*. Rijeka, Croatia: IntechOpen, 2020, ch. 5, pp. 75–94.

[6] M. Esposito et al., "Perspective on traveling wave microwave parametric amplifiers," *Appl. Phys. Lett.*, vol. 119, 2021, Art. no. 120501, doi: 10.1063/5.0061893.

[7] C. Guarcello et al., "Modeling of Josephson traveling wave parametric amplifiers," *IEEE Trans. Appl. Supercond.*, vol. 33, no. 1, Jan. 2023, Art. no. 0600207, doi: 10.1109/TASC.2022.3214751.

[8] R. Rousset-Zenou et al., "Gate-tunable Josephson parametric amplifiers based on semiconductor nanowires," 2025, *arXiv:2510.00305*.

[9] W. C. Stewart, "Current-voltage characteristics of Josephson junctions," *Appl. Phys. Lett.*, vol. 12, pp. 277–280, 1968, doi: 10.1063/1.1652260.

[10] D. E. McCumber, "Effect of AC impedance on DC voltage-current characteristics of superconductor weak-link junctions," *J. Appl. Phys.*, vol. 39, pp. 3113–3118, 1968, doi: 10.1063/1.1656743.

[11] A. Barone and G. Paternò, *Physics and Applications of the Josephson Effect*. Hoboken, NJ, USA: Wiley, 1982, doi: 10.1002/9783527612055.

[12] A. A. Golubov, M. Y. Kupriyanov, and E. Il'ichev, "The current-phase relation in Josephson junctions," *Rev. Mod. Phys.*, vol. 76, pp. 411–469, Apr. 2004, doi: 10.1103/RevModPhys.76.411.

[13] R. Citro, C. Guarcello, and S. Pagano, "Josephson junctions, superconducting circuits, and qubits for quantum technologies," in *New Trends and Platforms for Quantum Technologies, Lecture Notes in Physics*, vol. 1025, Cham: Springer, 2024, pp. 1–59, doi: 10.1007/978-3-031-55657-9_1.

[14] E. Goldobin et al., "Josephson junctions with second harmonic in the current–phase relation," *Phys. Rev. B*, vol. 76, 2007, Art. no. 224523, doi: 10.1103/PhysRevB.76.224523.

[15] E. Goldobin et al., "Josephson junction with a magnetic-field tunable ground state," *Phys. Rev. Lett.*, vol. 107, 2011, Art. no. 227001, doi: 10.1103/PhysRevLett.107.227001.

[16] H. Sickinger et al., "Experimental evidence of a φ Josephson junction," *Phys. Rev. Lett.*, vol. 109, 2012, Art. no. 107002, doi: 10.1103/PhysRevLett.109.107002.

[17] M. J. A. Stoutimore et al., "Second-harmonic current–phase relation in Josephson junctions with ferromagnetic barriers," *Phys. Rev. Lett.*, vol. 121, 2018, Art. no. 177702, doi: 10.1103/PhysRevLett.121.177702.

[18] A. G. P. Troeman et al., "Temperature dependence measurements of the supercurrent–phase relationship in niobium nanobridges," *Phys. Rev. B*, vol. 77, 2008, Art. no. 024509, doi: 10.1103/PhysRevB.77.024509.

[19] A. Chieppa et al., "Unveiling the current–phase relationship of InSb nanoflag Josephson junctions using a NanoSQUID magnetometer," *Nano Lett.*, vol. 25, pp. 14412–14419, 2025, doi: 10.1021/acs.nanolett.5c03765.

[20] C. Guarcello et al., "Driving a Josephson traveling-wave parametric amplifier into chaos," *Chaos Solitons Fractals*, vol. 189, 2024, Art. no. 115598, doi: 10.1016/j.chaos.2024.115598.

[21] R. Menditto et al., "Tunable φ Josephson junction ratchet," *Phys. Rev. E*, vol. 94, 2016, Art. no. 042202, doi: 10.1103/PhysRevE.94.042202.

[22] G. Singh et al., "Gate-tunable pairing channels in superconducting noncentrosymmetric oxide nanowires," *npj Quantum Mater*, vol. 7, 2022, Art. no. 2, doi: 10.1038/s41535-021-00401-2.

[23] P. Zhang et al., "Large second-order Josephson effect in planar superconductor–semiconductor junctions," *SciPost Phys.*, vol. 16, 2024, Art. no. 030, doi: 10.21468/SciPostPhys.16.2.030.

[24] A. Leblanc et al., "From nonreciprocal to charge-4e supercurrent in Ge-based Josephson devices," *Phys. Rev. Res.*, vol. 6, 2024, Art. no. 033281, doi: 10.1103/PhysRevResearch.6.033281.

[25] C. Ciaccia et al., "Charge-4e supercurrent in a two-dimensional InAs–Al heterostructure," *Commun. Phys.*, vol. 7, 2024, Art. no. 41, doi: 10.1038/s42005-024-01541-4.

[26] S. Messelot et al., "Direct measurement of a $\sin(2\varphi)$ current-phase relation," *Phys. Rev. Lett.*, vol. 133, 2024, Art. no. 106001, doi: 10.1103/PhysRevLett.133.106001.

[27] E. Il'ichev et al., "Phase dependence of the Josephson current in inhomogeneous high-Tc junctions," *Phys. Rev. B*, vol. 59, pp. 11502–11510, 1999, doi: 10.1103/PhysRevB.59.11502.

[28] E. Il'ichev et al., "Anomalous periodicity of the current-phase relationship," *Phys. Rev. B*, vol. 60, pp. 3096–3103, 1999, doi: 10.1103/PhysRevB.60.3096.

[29] D. Willsch et al., "Observation of Josephson harmonics in tunnel junctions," *Nature Phys.*, vol. 20, pp. 815–820, 2024, doi: 10.1038/s41567-024-02429-3.

[30] K. Bayros et al., "Influence of pinholes and weak-points in aluminum-oxide Josephson junctions," *Phys. Rev. Mater.*, vol. 8, 2024, Art. no. 046202, doi: 10.1103/PhysRevMaterials.8.046202.

[31] J. Griesmar et al., "Aluminum junctions with well-transmitted channels," *Phys. Rev. Appl.*, vol. 24, 2025, Art. no. 064065, doi: 10.1103/PhysRevApplied.24.064065.

[32] T. J. Maldonado et al., "Mesoscopic theory of the Josephson junction," *Phys. Rev. B*, vol. 111, 2025, Art. no. L140505, doi: 10.1103/PhysRevB.111.L140505.

[33] C. Guarcello et al., "Effect of a second-harmonic current–phase relation," *Appl. Phys. Lett.*, vol. 126, 2025, Art. no. 162602, doi: 10.1063/5.0262555.

[34] H. Haider, "A black-box quantum model for superconducting traveling-wave parametric amplifiers," *IEEE Trans. Microw. Theory Techn.*, vol. 72, no. 4, pp. 2143–2157, Apr. 2024, doi: 10.1109/TMTT.2023.3345641.

[35] C. Guarcello et al., "Nonlinear behavior of Josephson traveling wave parametric amplifiers," *IEEE Trans. Appl. Supercond.*, vol. 34, no. 3, May 2024, Art. no. 1701105, doi: 10.1109/TASC.2024.3367615.

[36] Wolfram Research, Inc., *Mathematica*, Version 14.3, Champaign, IL, 2025, https://www.wolfram.com/mathematica

[37] S. T. Elkin, M. Haider, and T. E. Roth, "Multiphysics numerical method for modeling Josephson traveling-wave parametric amplifiers," *IEEE J. Multiscale Multiphys. Comput. Tech.*, vol. 9, pp. 247–257, 2024, doi: 10.1109/JMMCT.2024.3428344.

[38] O. Yaakobi et al., "Parametric amplification in Josephson junction embedded transmission lines," *Phys. Rev. B*, vol. 87, 2013, Art. no. 144301, doi: 10.1103/PhysRevB.87.144301.

[39] K. O'Brien et al., "Resonant phase matching of Josephson traveling-wave parametric amplifiers," *Phys. Rev. Lett.*, vol. 113, 2014, Art. no. 157001, doi: 10.1103/PhysRevLett.113.157001.

[40] S. Ó. Peatáin et al., "Simulating fabrication tolerance effects," *Supercond. Sci. Technol.*, vol. 36, 2023, Art. no. 045017, doi: 10.1088/1361-6668/acba4e.

[41] T. C. White et al., "Traveling-wave parametric amplifier with Josephson junctions," *Appl. Phys. Lett.*, vol. 106, 2015, Art. no. 242601, doi: 10.1063/1.4922593.

[42] C. Macklin et al., "A near-quantum-limited Josephson traveling-wave parametric amplifier," *Science*, vol. 350, pp. 307–310, 2015, doi: 10.1126/science.aaa8525.

[43] M. Engelhardt, LTspice/SwitcherCAD III, Linear TechnologyCorporation, https://www.analog.com, 2007.

[44] C. M. Caves, "Quantum limits on noise in linear amplifiers," *Phys. Rev. D*, vol. 26, no. 8, pp. 1817–1839, 1982, doi: 10.1103/PhysRevD.26.1817.

[45] A. L. Grimsmo and A. Blais, "Squeezing and quantum state engineering," *npj Quantum Inf.*, vol. 3, 2017, Art. no. 20, doi: 10.1038/s41534-017-0024-0.

Open Access funding provided by 'Università degli Studi di Salerno' within the CRUI CARE Agreement